Decadal and Seasonal Dependence of ENSO Prediction Skill

MAGDALENA A. BALMASEDA

Departamento de Fisica, Universidad de Alcala de Henares, Alcala de Henares, Madrid, Spain

MICHAEL K. DAVEY

Hadley Centre, U.K. Meteorological Office, Bracknell, Berkshire, England

DAVID L. T. ANDERSON

Atmospheric, Oceanic and Planetary Physics, University of Oxford, Oxford, England

(Manuscript received 19 October 1994, in final form 17 April 1995)

ABSTRACT

When forecasting sea surface temperature (SST) in the Equatorial Pacific on a timescale of several seasons, most prediction schemes have a spring barrier; that is, they have skill scores that are substantially lower when predicting northern spring and summer conditions compared to autumn and winter. This feature is investigated by examining predictions during the 1970s and the 1980s, using a dynamic ocean model of intermediate complexity coupled to a statistical atmosphere. Results show that predictions initialized during the 1970s exhibit the typical prominent skill decay in spring, whereas the seasonal dependence in those predictions initialized during the 1980s is rather small. Similar changes in seasonal dependence are also found in predictions based on simple persistence of observed SST anomalies.

This decadal change in the spring barrier is related to decadal variations found in the seasonal phase locking of the SST anomalies, which is largely determined by the timing of El Niño events. The spring barrier was strong in the 1970s, when El Niño was strongly phaselocked to the annual cycle. An analysis of observed SST anomalies from 1900 to 1990 shows several changes in behavior on a decadal scale, with the largest change being from the 1970s to the 1980s.

The seasonal dependence of model heat content predictions is investigated and found to be similar to that for SST, except that it shows a winter barrier rather than the spring barrier evident in SST.

1. Introduction

In the last decade, considerable progress has been made in the understanding and prediction of the El Niño/Southern Oscillation (ENSO) phenomenon, which is the main climate fluctuation at interannual timescales in the tropical Pacific. The results of both numerical modeling and data analysis have shed light on the mechanisms that drive the aperiodic alternation between the cold and warm phases of ENSO (McCreary and Anderson 1991; Neelin et al. 1994). A hierarchy of prediction schemes, ranging from pure statistical models to sophisticated coupled GCMs, has been developed: claims are made that ENSO can be successfully predicted up to one year in advance (Latif et al. 1994).

One prominent feature of the predictions of sea surface temperature (SST) anomalies associated with ENSO, common to most of the models, is a pronounced seasonal variation in skill. Many prediction schemes show a marked decay in skill during northern spring (the "spring barrier"), followed sometimes by a recovery of skill in autumn and winter. The causes and nature of the seasonal dependence still remains as an open question. Some authors (Zebiak and Cane 1987; Battisti 1988; Goswami and Shukla 1991) have discussed the seasonal dependence of predictability in their models, concluding that the predictability of the system is smaller during spring because the interaction between the ocean and the atmosphere that drives interannual anomalies is weaker during this season; this explanation has been supported by results with empirical models, such as the seasonal principal oscillation pattern analysis carried out by Blumenthal (1991). Webster and Yang (1992) have used observed circulation features to investigate the predictability barrier, and they suggest that interaction with the rapid spring development of the south Asian summer monsoon may be a factor. As shown by Xue et al. (1994), the spring

Corresponding author address: Dr. Michael K. Davey, Hadley Centre for Climate Prediction and Research, Meteorological Office, London Road, Bracknell, Berkshire RG12 2SZ, United Kingdom.
E-mail: mkdavey@meto.govt.uk

barrier in skill can also be due to the seasonality of SST anomaly variance: low spring variance decreases correlation skill at that time, with apparent skill recovery in subsequent seasons when variance is higher.

There is evidence (Gill and Rasmusson 1983; Kousky and Leetmaa 1989; Wang 1995) that the warm events during the 1980s are different, both in spatial distribution and timing, when compared to the canonical El Niño event described by Rasmusson and Carpenter (1982) for composites of earlier El Niño events. Motivated by these results, we try to address three main questions, by using predictive skill scores and statistical analysis of observations: (a) how does predictability differ in the 1970s and the 1980s; (b) are these differences related to the phase relationship between ENSO and the seasonal cycle; (c) do these differences constitute an isolated episode or are they linked to changes occurring at interdecadal timescales?

An intermediate dynamical ocean-empirical atmosphere coupled model was used to conduct prediction experiments during the 1970s and 1980s, as described in section 2. Systematic differences in the prediction scores between the two decades are found (section 3). Predictions made using simple persistence of observed SST anomalies, described in section 4, exhibit similar decadal differences. Further analysis suggests that differences in ENSO during the 1970s and 1980s are closely related to the relation of ENSO to the seasonal cycle. Interdecadal changes from the beginning of this century are also analyzed and discussed in section 4, using observed SST.

2. Dynamical prediction experiments

Predictions were carried out using the coupled model described in Balmaseda et al. (1994), which consists of a tropical Pacific Ocean model with two active layers coupled to a statistical model that relates SST anomalies and surface wind stress anomalies. (The anomalies are relative to monthly climatology.) The ocean model is first forced by observed wind stress (based on data from The Florida State University, Goldenberg and O'Brien 1981) during the period 1961–1991. The output of this simulation run is used to build the statistical atmosphere model, which assumes that the wind stress anomalies are a linear function of the first six principal components of the model SST anomalies, with seasonal variation. Figure 1 shows the time series of model-simulated monthly anomalies SST'_{sim} for the east-central Pacific Niño3 region (5°N–5°S, 150°–90°W), where $'$ denotes perturbations from monthly climatology. The model represents observed interannual variations well. The simulation is described in more detail in Balmaseda et al. (1994).

The initial conditions for 92 hindcast experiments, each of 24 months duration, are taken from the simulation run at 3-month intervals (1 January, 1 April, 1 July, 1 October) during the period 1969–1991. Cor-

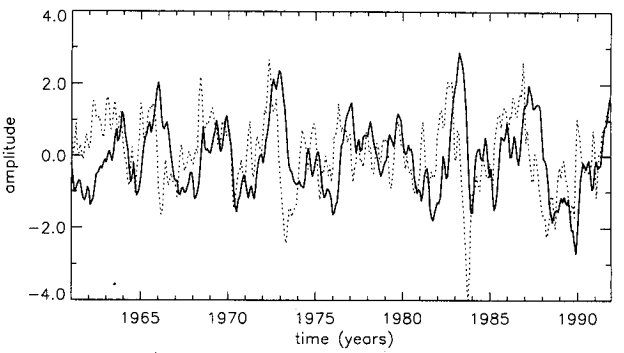

FIG. 1. Niño3 SST′ (solid) and equatorial band HC′ (dashed), from the ocean model simulation of the tropical Pacific forced by observed winds from 1961 to 1992. The time series are normalized by the standard deviations 0.69°C (SST′) and 0.16°C (HC′).

relation skill scores r are used to evaluate the model predictions. For example, $r(SST'_{pred}, SST'_{obs})$ will denote the correlation of a set of model-predicted values of SST'_{pred} with observed values of SST'_{obs}. The observations of SST are taken from the UKMO Global Ice and Sea Surface Temperature (GISST) dataset (Parker et al. 1994). The observed climatology is the 1951–1980 GISST average. This dataset has the advantage of going back beyond the beginning of this century, which is needed for the analysis of interdecadal variability in section 4. All the analyses concerning the last two decades have also been repeated with the Comprehensive Oceanic and Atmospheric Data Set (COADS, Woodruff et al. 1987). There are no significant differences between the results obtained with the two datasets for this time period.

The correlations $r(SST'_{pred}, SST'_{obs})$ as a function of lead time for all hindcasts are shown in Fig. 2a for the Niño 3 region, where the model performance is good and comparable to other models (Latif et al. 1994). Figure 2b shows $r(SST'_{pred}, SST'_{obs})$ for hindcasts separated according to the season at the *start* of each hindcast; clearly the predictive skill of the coupled system has a strong seasonal dependence. In agreement with other models (e.g., that of Zebiak and Cane 1987), the correlation skill of the predictions decreases markedly as hindcasts pass through northern spring. Predictions initialized in spring show stable behavior for one year, with skill declining when predicting conditions for the next spring, reaching a minimum when predicting summer. The skill of predictions starting in summer declines after 9 months, when predicting spring conditions, and so on. For comparison, seasonally separated correlations $r(SST'_{pred}, SST'_{sim})$ of hindcasts against the model simulation are shown in Fig. 2c. The spring barrier is somewhat weaker than in Fig. 2b, but is still evident. [Note that the correlations in Fig. 2b at zero lead time measure $r(SST'_{sim}, SST'_{obs})$, which is about 0.7 for autumn, and about 0.8 for the other seasons. The correlations of model hindcasts against model sim-

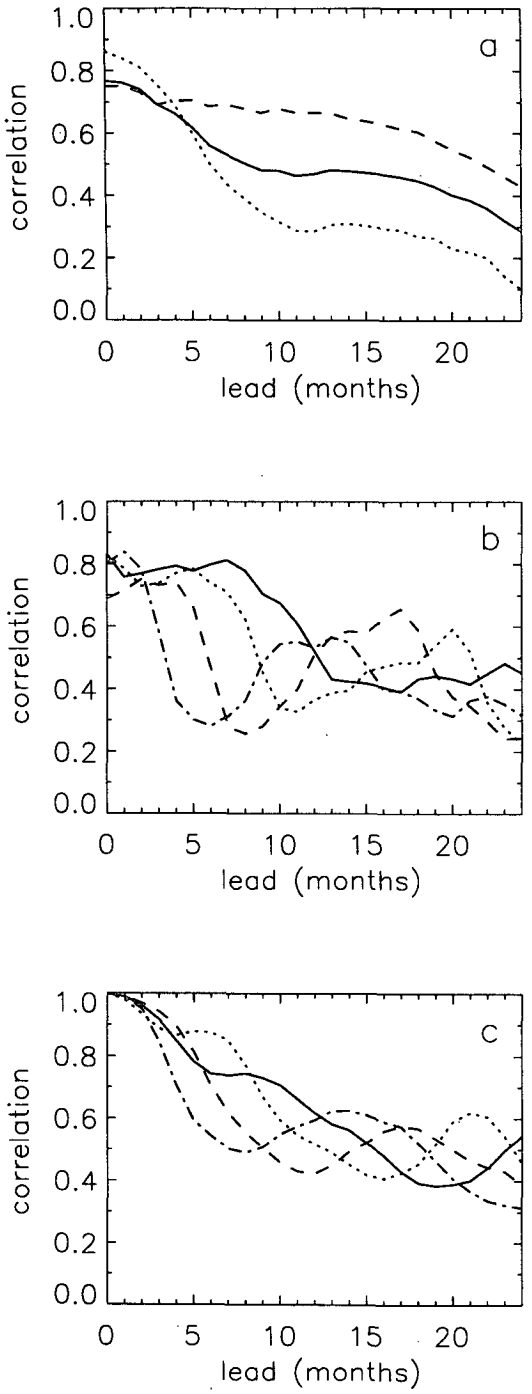

FIG. 2. Correlations r of observed, simulated, and predicted (dynamical model) Niño3 anomalies SST′, as a function of lead time. Predictions are made at 3-month intervals. (a) Shows $r(\mathrm{SST}'_{\mathrm{pred}}, \mathrm{SST}'_{\mathrm{obs}})$ using data from the periods 1970–1990 (solid), 1970–1980 (dotted), and 1980–1990 (dashed). (b) Shows $r(\mathrm{SST}'_{\mathrm{pred}}, \mathrm{SST}'_{\mathrm{obs}})$ using data from 1970 to 1990, separated according to the season when the model prediction was initialized and started: in northern spring (solid), summer (dotted), autumn (dashed), and winter (dot–dashed). (c) Shows $r(\mathrm{SST}'_{\mathrm{pred}}, \mathrm{SST}'_{\mathrm{sim}})$ using data from 1970 to 1990, separated according to the season when the model prediction was initialized and started: in northern spring (solid), summer (dotted), autumn (dashed), and winter (dot–dashed).

ulation values in Fig. 2c must be unity at zero lead time.]

Other skill measures were calculated, in particular, root mean square error (rmse), and root-mean-square error with the forecast and target values normalized by their respective month-of-year standard deviations (rmsn). In general, the skill as measured by rmsn was found to be very similar to correlation skill, in that rmsn is low when r is high, and the same seasonal features are evident. For $\mathrm{SST}'_{\mathrm{pred}}$ and $\mathrm{SST}'_{\mathrm{sim}}$ differences, rmse was similar to rmsn. For $\mathrm{SST}'_{\mathrm{pred}}$ and $\mathrm{SST}'_{\mathrm{obs}}$ differences, there was a clear spring rmse minimum that was much less prominent in rmsn.

Changes in upper-ocean equatorial heat content are another important component of tropical ocean variability, closely related to wind and SST changes. Heat content anomalies have been used to predict SST′ usefully (e.g., Latif and Graham 1992; Balmaseda et al. 1994). Here we consider the predictability of heat anomalies using the present dynamical model. The heat content is defined as the temperature vertically integrated over the two active layers of the ocean model (about 275 m), scaled by mean depth to give units of temperature. In particular, the heat content anomalies HC′ in the Pacific-wide equatorial band 5°N–5°S are considered. (Equatorial band HC′ is chosen because, unlike SST′, which is concentrated in the east-central Pacific, HC′ variability is spread throughout the equatorial Pacific.) The time series of $\mathrm{HC}'_{\mathrm{sim}}$ is included in Fig. 1. The lag correlation of model $\mathrm{HC}'_{\mathrm{sim}}$ and $\mathrm{SST}'_{\mathrm{sim}}$ in Fig. 3 confirms that these variables are closely related, with largest positive r at a lead of 4 to 5 months, with HC′ leading SST′.

Hindcasts $\mathrm{HC}'_{\mathrm{pred}}$ of HC anomalies are validated only against values $\mathrm{HC}'_{\mathrm{sim}}$ from the model simulation forced by observed winds, because we do not have reliable observations of heat content for the 23-year period considered. Figure 4 shows correlations $r(\mathrm{HC}'_{\mathrm{pred}}, \mathrm{HC}'_{\mathrm{sim}})$ as a function of lead time, separated by season: r exceeds 0.6 for lead times of up to 10 months. Like Niño3 SST′, model HC′ correlation skill has seasonal dependence (weaker than for SST′), and can partially recover after a decline. A feature of Fig. 4 compared to Fig. 2c is that the decline in HC′ correlation occurs about one season before the decay in the SST′ skill: there is a winter barrier instead of a spring barrier. This timing is consistent with the lag relation in Fig. 3.

After the spring (winter) decrease, the SST′ (HC′) correlations often increase with lead time. The rapid decline and subsequent recovery can be partly an artifact of the skill measure used, for example, because variance depends on the month-of-year (Xue et al. 1994). For $\mathrm{SST}'_{\mathrm{sim}}$ the month-of-year variance for 1970–90 has a winter maximum followed by a decline into spring that would help account for the spring drop in correlations (Fig. 2c). The $\mathrm{SST}'_{\mathrm{sim}}$ variance then remains relatively low through summer and autumn. The month-of-year variance of $\mathrm{HC}'_{\mathrm{sim}}$ similarly has a weak

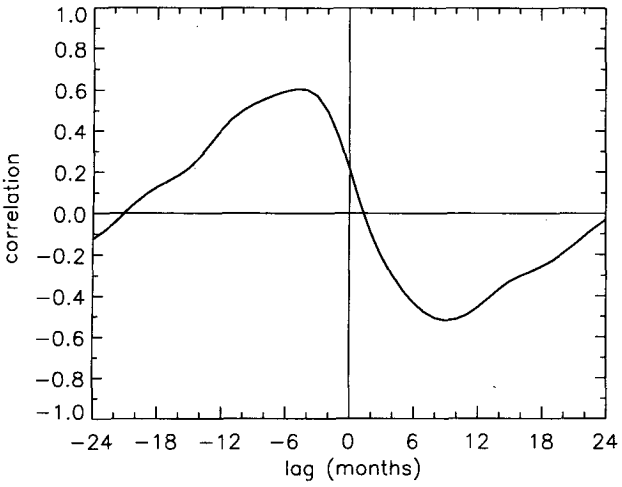

FIG. 3. Lag correlation of Niño3 SST′ with equatorial band HC′, from the ocean model simulation of the tropical Pacific, forced by observed winds from 1961 to 1992. For negative lag, HC′ leads SST′.

autumn maximum followed by a winter minimum. Neither SST'_{sim} nor HC'_{sim} has a sharp variance increase following the minimum, however.

The recovery of skill after a decline may also have a physical explanation if whatever causes the loss of predictability at that time does not completely destroy the memory of the coupled system. The disturbance causing the drop in SST predictability might be a surface phenomenon that does not likewise influence the subsurface structure of the ocean at the same time. Thus, the system could keep part of the overall structure that determines its slow evolution, and its components could recover skill, provided that the disturbance does not affect the surface and subsurface structure simultaneously. The phase difference between HC′ and SST′ in the drop and recovery of predictive skill suggests that surface and subsurface information is indeed not lost simultaneously. A possible scenario is that when HC′ skill declines, SST′ can drive wind anomalies that force HC′ changes that allow recovery of HC′ skill; and when SST′ skill falls, HC′ can cause upwelling changes that allow recovery of SST′ skill.

3. Decadal contrasts

The dynamical prediction experiments were next separated into two subsets: predictions initialized during the decade of 1970–1980, and predictions initialized during the decade 1981–1990. (It makes little difference to the results if the subsets are divided elsewhere in the range 1978 to 1981.) The separate 1970s and 1980s correlations $r(SST'_{pred}, SST'_{obs})$ included in Fig. 2a show that there is a clear difference between the two decades for predictions of observed Niño3 SST′, with higher scores during the 1980s at lead times longer than 6 months. (Remarkably, r is larger than 0.6 for lead times of up to 18 months in the 1980s.) The seasonal dependence of correlations for Niño3 SST′ also differs greatly in the 1970s and 1980s, as shown in Fig. 5 for $r(SST'_{pred}, SST'_{obs})$ and in Fig. 6 for $r(SST'_{pred}, SST'_{sim}$. For the 1970s (Figs. 5a, 6a) r decreases rapidly in spring, reaching a minimum in summer. The correlations always recover after the pronounced decay. The amplitude of the seasonal dependence is large, remarkably so for $r(SST'_{pred}, SST'_{obs})$. By contrast, Figs. 5b, 6b for the 1980s show small seasonal dependence of r.

Figure 7 likewise shows seasonal $r(HC'_{pred}, HC'_{sim})$ for the prediction of model equatorial band HC′ for the 1970s and 1980s. Again there is a strong prediction barrier in the 1970s (in winter for HC′), but not in the 1980s. From Figs. 6a and 7a the phase lag of one season between HC′ and SST′ correlations is again evident in the 1970s.

There are also clear seasonal differences in variability for the 1970s and 1980s. Figure 8 shows time series of January, April, July, and October observed Niño3 SST′, together with dynamical model predictions initialized 9 months in advance. The observed SST′ values are particularly low in April during the 1970s, and the predictions do not reproduce such a low amplitude. [These small April anomalies are also difficult to simulate, as demonstrated by the low $r(SST'_{pred}, SST'_{obs})$ values in Fig. 5a at zero lead in spring.] The variance of observed SST′ organized by month-of-year is shown in Fig. 9 for the decades of the 1970s and 1980s. The 1970s and 1980s each have a winter maximum, but in the 1970s the variability has a pronounced minimum in March–April–May, which is much less prominent during the 1980s. (Note: when examined separately, cold and warm anomalies show the same behavior.)

Similarly, month-of-year Niño3 SST′ variances calculated from the model simulation have winter max-

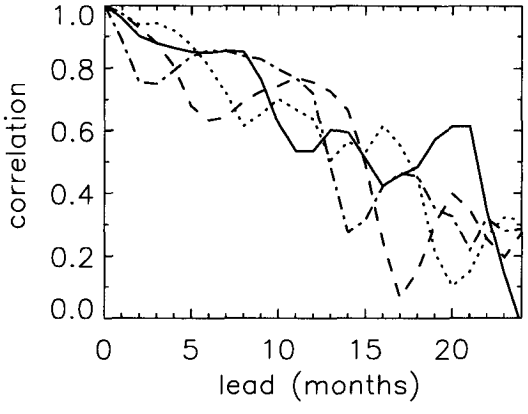

FIG. 4. Correlation $r(HC'_{pred}, HC'_{sim})$, using equatorial band HC′ data from 1970 to 1990, separated according to the season when the model prediction was initialized and started: in northern spring (solid), summer (dotted), autumn (dashed), and winter (dot–dashed).

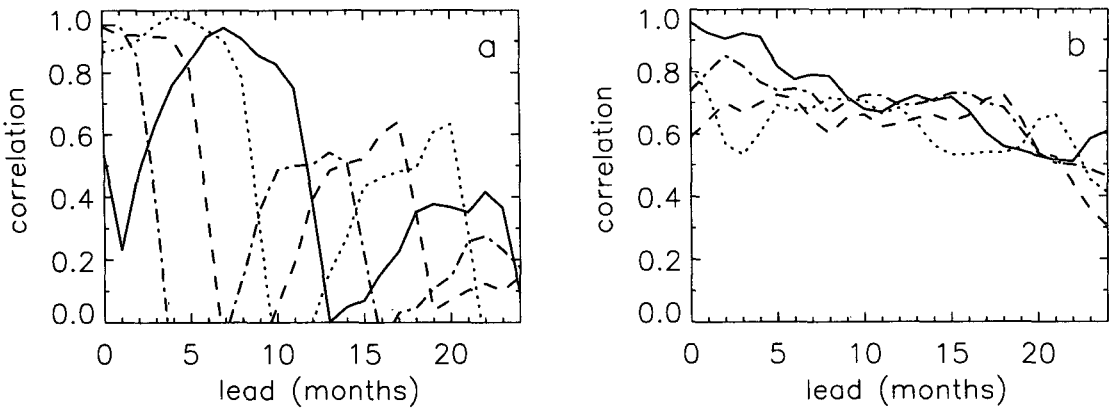

FIG. 5. Correlations $r(\mathrm{SST}'_{\mathrm{pred}}, \mathrm{SST}'_{\mathrm{obs}})$ of predicted (dynamical model) and observed Niño3 SST′, as a function of lead time. Predictions are made at 3-month intervals. Data separated according to the season when the model prediction was initialized and started: in northern spring (solid), summer (dotted), autumn (dashed), and winter (dot–dashed): (a) data from the 1970s, (b) data from the 1980s.

ima, a distinct May–June minimum in the 1970s, and no clear minimum in the 1980s. For model equatorial band HC′ variances, there is no clear minimum in the 1970s or 1980s, a May maximum in the 1970s and an October maximum in the 1980s.

During the 1970s interannual variability was strongly phase locked to the seasonal cycle, with the transition phase of El Niño (anomalies near zero) occurring in spring in region Niño3. That would explain the low spring variability of the anomalies and the spring drop in the correlation skill when passing from one phase of El Niño to the other. During the 1980s, however, there seems not to be a preferred season for the El Niño transition phase, and the variance of the anomalies does not exhibit a pronounced minimum in spring. This scenario agrees with the description by Wang (1995) of the changes in the onset of the warm phase of El Niño before and after the late 1970s.

4. Analysis of observations

a. Simple persistence for the 1970s and 1980s

We first corroborate the results of the model predictions by using simple persistence of the observed SST anomalies to compute analogous skill scores for the same cases. Initial anomalies are held constant throughout the prediction period to obtain estimates $\mathrm{SST}'_{\mathrm{per}}$. Correlations $r(\mathrm{SST}'_{\mathrm{per}}, \mathrm{SST}'_{\mathrm{obs}})$ for Niño3 SST′ with initial conditions over the 1970s and over the 1980s are shown in Fig. 10a: skill is clearly higher in the 1980s, as was found for the dynamical model predictions (cf. Fig. 2a). Corresponding correlations separated by initial season are also provided in Fig. 10. During the 1970s (Fig. 10b) seasonal dependence is strong: persistence is a good predictor until spring, when there is a very rapid decline in r. In the 1980s (Fig. 10c) the seasonal dependence is weaker, and the decay that oc-

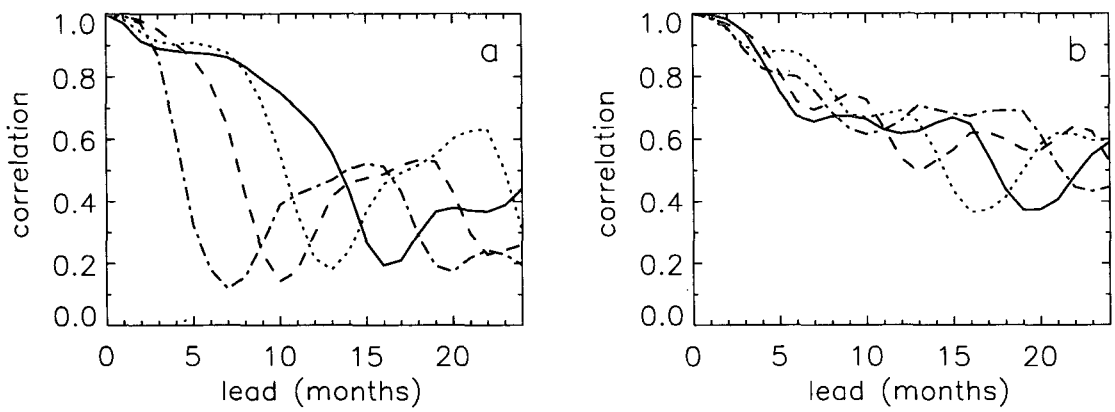

FIG. 6. Correlations $r(\mathrm{SST}'_{\mathrm{pred}}, \mathrm{SST}'_{\mathrm{sim}})$ of predicted (dynamical model) and simulated Niño3 SST′, as a function of lead time. Predictions are made at 3-month intervals. Data separated according to the season when the model prediction was initialized and started: in northern spring (solid), summer (dotted), autumn (dashed), and winter (dot–dashed): (a) data from the 1970s, (b) data from the 1980s.

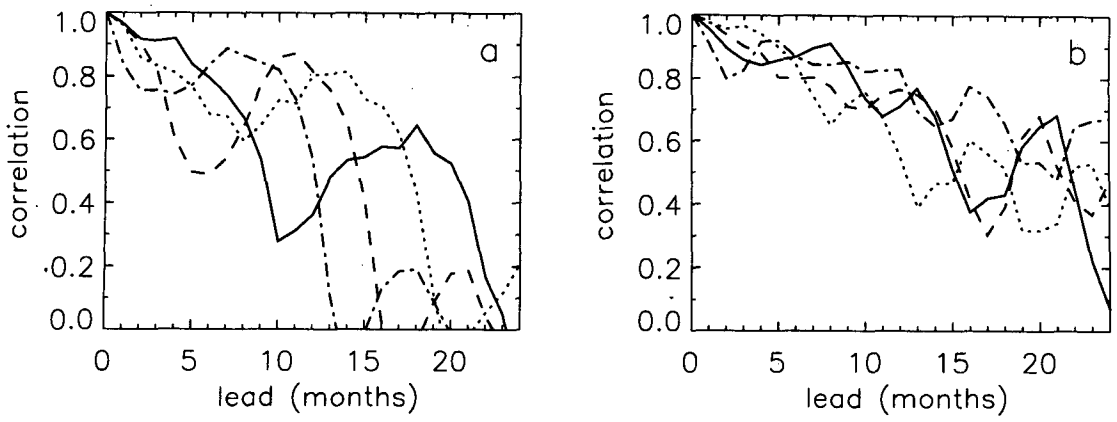

FIG. 7. Correlations $r(HC'_{pred}, HC'_{sim})$ of predicted (dynamical model) and simulated equatorial band HC′, as a function of lead time. Predictions are made at 3-month intervals. Data separated according to the season when the model prediction was initialized and started: in northern spring (solid), summer (dotted), autumn (dashed), and winter (dot–dashed): (a) data from the 1970s, (b) data from the 1980s.

curs in summer/autumn is not as sharp. (Note that persistence skill is high for about 8 months for 1970s summer and 1980s autumn starts.) In contrast to the dynamical model results, the persistence correlations do not recover substantially after a sharp decline.

Similar calculations of the persistent behavior of SST anomalies has been repeated for anomalies in different regions of the Pacific. Compared to Niño3, there is hardly any seasonality in the Western Pacific (Niño4), but there is stronger seasonality (and decadal differences) toward the east (regions Niño1 and 2).

It seems then that there are clear differences between the interannual variability of the decades of the 1970s and 1980s. These differences could be related to a dramatic change in the mean state of the climate system that occurred during 1977–1978, in which large changes were noticed in the Tropics and the extratropics (Trenberth 1990; Kerr 1992; Trenberth and Hurrell 1994).

b. *Interdecadal changes*

The question arises as to whether such decadal changes have occurred at other times. One main obstacle to answering this question is the availability of observations. The UKMO GISST dataset provides gridded values that go back beyond the beginning of this century, but the spatial coverage of actual observations has changed considerably with time. However, averaging over relatively large areas provides a method of improving the quality of the records, at the expense of a decreased spatial resolution. Figure 11 shows SST′ in region Niño3 for this century, showing the main ENSO events that occurred irregularly throughout this period. [Note: a new GISST dataset is in preparation for which empirical orthogonal functions are used to improve the estimates of SST in data-sparse regions (Rayner et al. 1995, personal communication.)]

We will focus attention on two features of the interannual variability of SST that may be affected by interdecadal changes: persistence of SST in the Niño3 region, and seasonal variations of the interannual variance. We have defined indices P and V to represent these features. For each month-of-year m, indices $P(y_0, m)$ and $V(y_0, m)$ use information in a window centered on year y_0 ($y_0 = 1$ corresponds to 1901, etc.). The window covers 15 years ($y_0 - 7$ to $y_0 + 7$), with values in the outer 2 years at each end tapered by cosine tails. (The cosine tails simply smooth abrupt changes, and do not qualitatively affect the results.) Anomalies denoted T'' are relative to the mean within the window. The index P is the correlation of Niño3 anomalies (denoted T''_3) with values 3 months before (i.e., the correlation skill of simple persistence at a lead of 3 months). Index V is a measure of the variance within the window:

$$V(y_0, m) = \cdot \sum_{y=y_0-7}^{y_0+7} T''_3(12y + m)^2 W(y - y_0) \Big/ \sum_{y_0-7}^{y_0+7} W(y - y_0), \quad (1)$$

where $W \leqslant 1$ is the window factor, y_0 ranges from 7 to 85, and m ranges from 1 to 12.

Large (small) values of P in a particular season indicate that T''_3 systematically changes slowly (rapidly) at that time of year within the decadal window. Large dependence of P on month-of-year is a sign of a seasonal prediction barrier. Large changes in V with month-of-year indicate strong phaselocking of anomalies to the annual cycle, within the current window.

Figure 12 shows the values of P and V since the beginning of this century. In the 1970s and 1980s, P and V demonstrate the features discussed above. In the 1970s P has large seasonality with a promi-

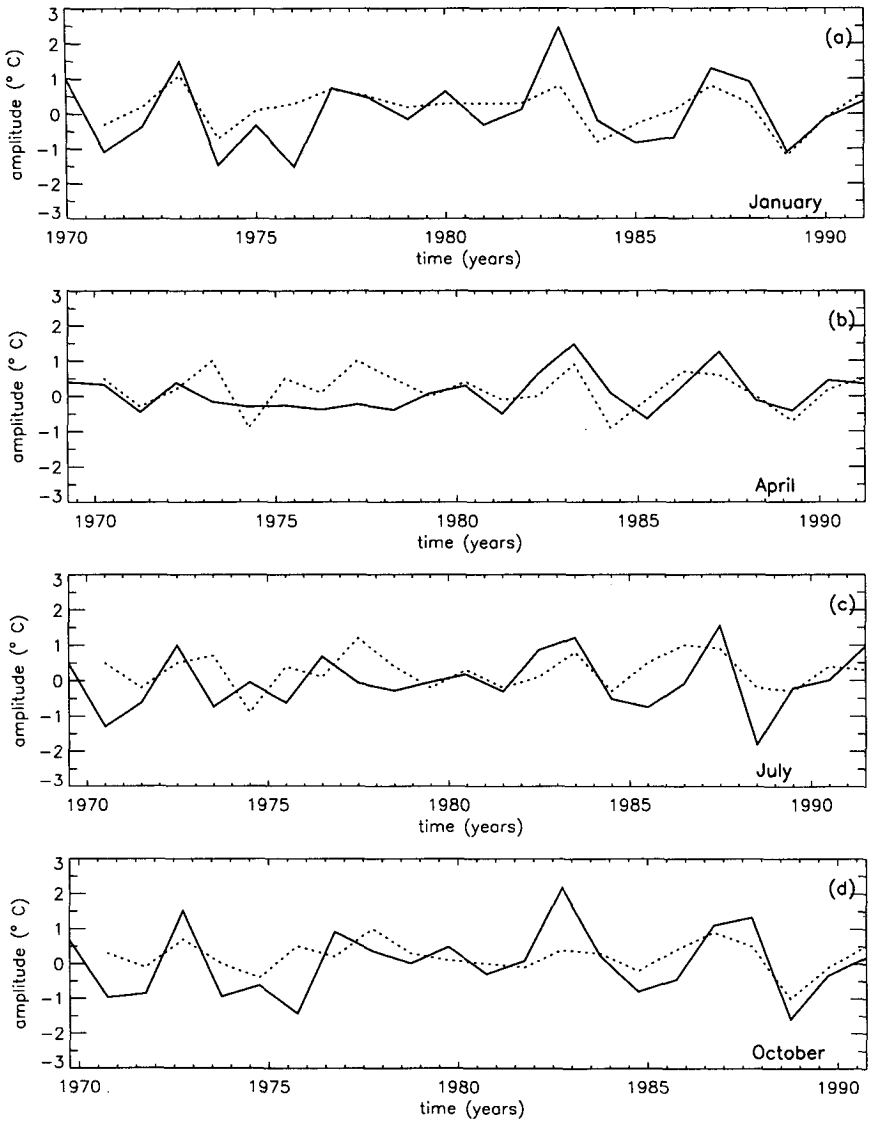

FIG. 8. Observed (solid line) and predicted (from dynamical model initialized 9 months before, dotted line) Niño3 SST′ for 1970–1991: (a) January values, (b) April, (c) July, and (d) October. Note the low amplitude of the observed April anomalies during the 1970s.

nent spring barrier: an autumn/winter maximum is followed by a sharp decline to a minimum when predicting spring conditions. When 1980s information dominates the window there is a switch to low seasonality, with P larger on average than in the 1970s. In the 1980s P has a winter maximum and autumn minimum, but is irregular through the rest of the year. In the 1970s V has large seasonality, with a sharp decrease from winter to spring followed by gradual recovery, giving a sawtooth profile. By contrast, in the 1980s V seasonality is lower and there are both spring and autumn minima. (The shape of index V in the mid-1970s and mid-1980s reproduces the month-of-year variances in Fig. 9.)

Generally, P and V have winter maxima, with a rapid decline in V going into spring. Several changes in P and V behavior in this century are also apparent in Fig. 12, with relatively abrupt (i.e., in 2 or 3 years) shifts followed by stable behavior for about 10 years. Early this century V and P have moderate seasonal range, with summer minima. Around 1916 there is a shift to exceptionally low V, and irregular P seasonality with a strong semiannual component. (This new behavior is not due to the absence of interannual variability, but rather is due to lack of seasonal phase locking. In Fig. 11 it can be seen that several cold events occurred in 1915–25, but each extremum occurred in a different season.)

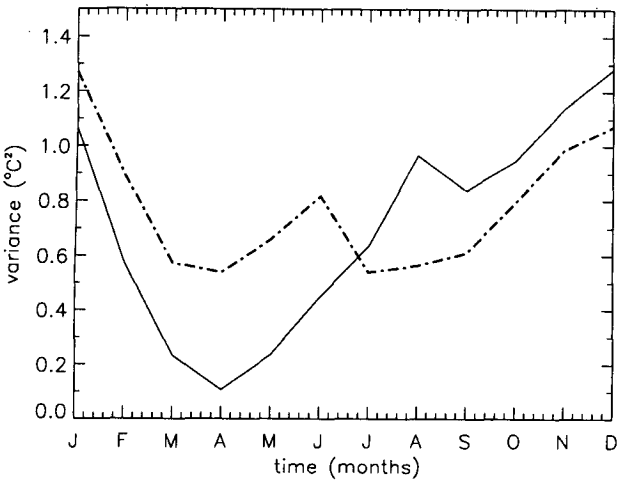

FIG. 9. Variance of observed Niño3 SST′ as a function of month-of-year, calculated for the 1970s (solid line) and the 1980s (dash–dot).

Around 1926 there is shift back to a regime like the early 1900s. Then around 1936 P decreases and is very irregular for a couple of years: in Fig. 11 it can be seen that this is a period of low interannual variability. During the 1940s P has larger seasonal range, with a near-zero minimum that varies between autumn and spring. Then in the late 1940s there is a shift to irregular P with low seasonality, as found in the 1920s (and 1980s). In the late 1950s there is a return to large P seasonality that lasts through the 1960s and 1970s. In terms of the seasonal range of V and P, the largest values this century occur in the 1970s.

5. Summary and discussion

Predictions of SST anomalies in region Niño3 for 1979–91, from a coupled model with a dynamical ocean component, were analyzed. The correlation skill shows a pronounced drop during spring conditions, often followed by a substantial recovery. This spring barrier is accompanied by a spring decline in SST′ variance. Other skill measures, such as normalized rms error, show similar seasonal dependence.

Predictions of oceanic equatorial band heat content anomalies HC′ were also considered. Correlation skill for HC′ tends to decay in winter and then partially recover: that is, there is a winter barrier that precedes the SST′ spring barrier. The timing is consistent with the tendency for HC′ to lead Niño3 SST′ by a few months.

Correlation skill decline and recovery can be due to seasonal changes in variance, because low variance tends to decrease correlations. Such variance changes can be substantial if, for example, the El Niño cycle is closely related to the annual cycle. Skill recovery may be assisted by a physical mechanism, if HC and SST

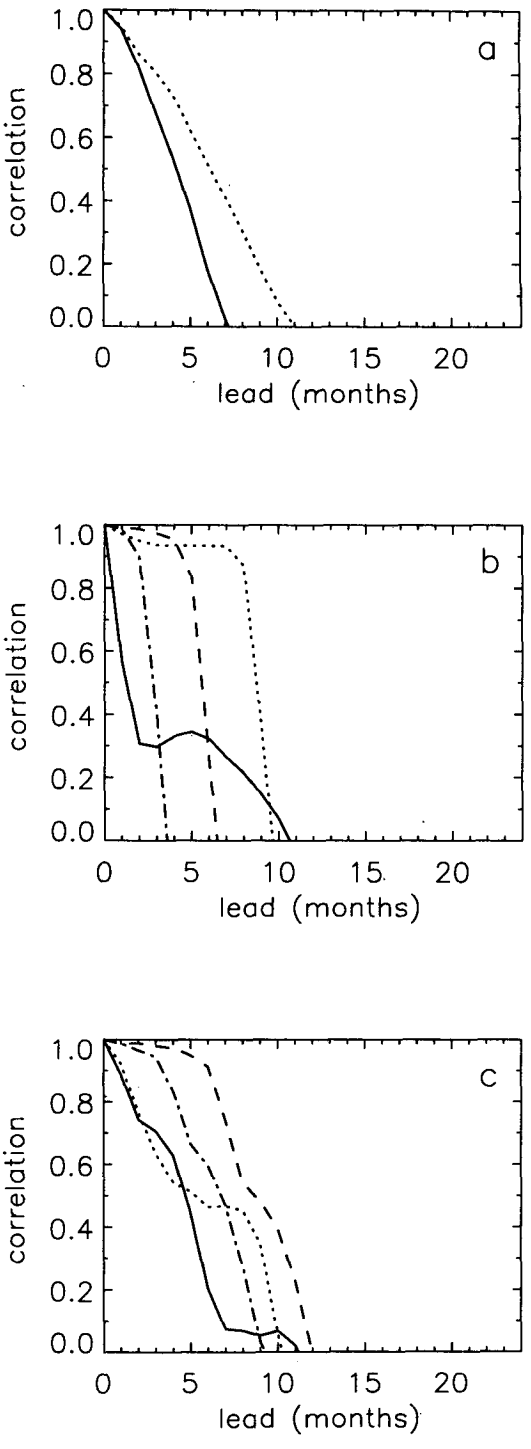

FIG. 10. Correlations $r(\mathrm{SST}'_{\mathrm{per}}, \mathrm{SST}'_{\mathrm{obs}})$ of observed and predicted (simple persistence) Niño3 SST′, as a function of lead time. Predictions are made at 3-month intervals. (a) All data from the periods 1970–1980 (solid) and 1980–1990 (dotted). (b) Data from the 1970s separated according to the season when the persistence prediction was started: in northern spring (solid), summer (dotted), autumn (dashed), and winter (dot–dashed). (c) Data from the 1980s separated according to the season when the persistence prediction was started: in northern spring (solid), summer (dotted), autumn (dashed), and winter (dot–dashed).

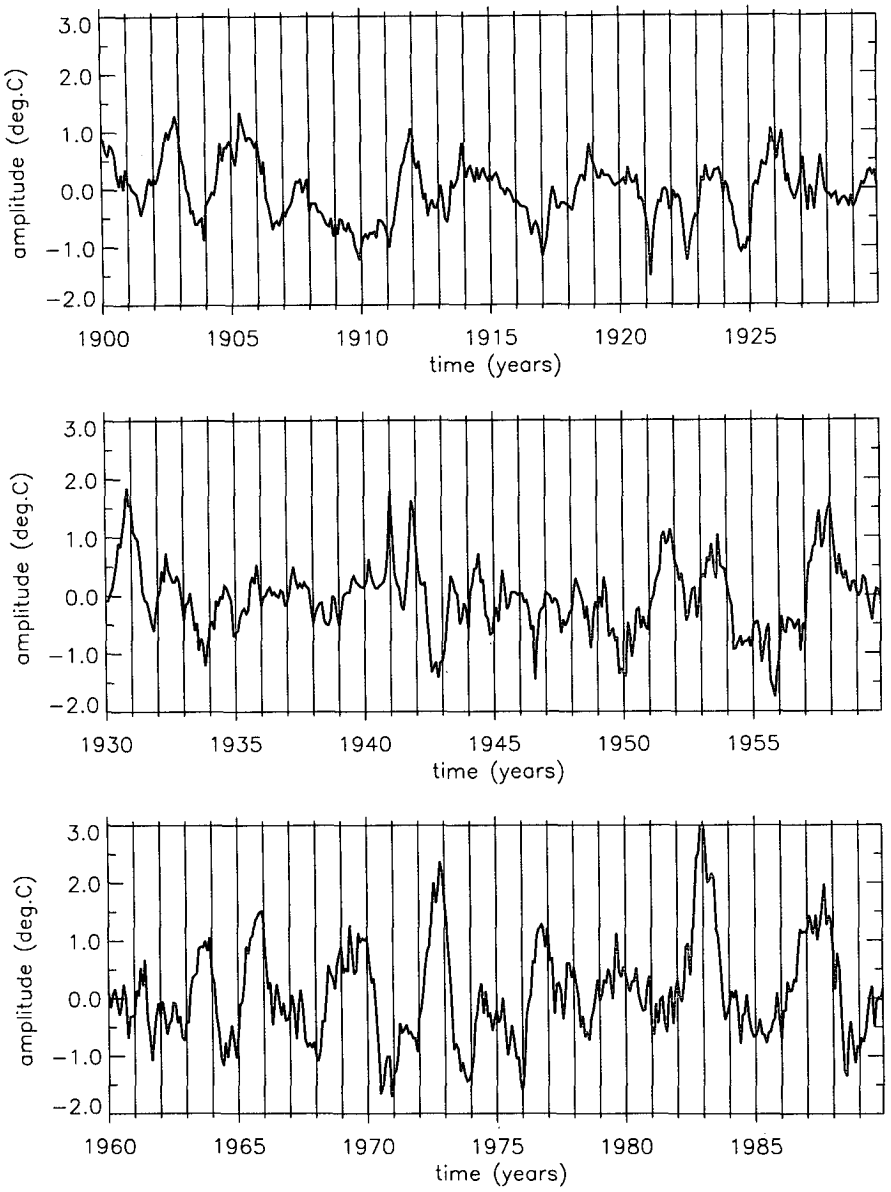

FIG. 11. Observed Niño3 SST′ for 1900 to 1990. Vertical lines correspond to the start of each year.

information is not lost simultaneously and the coupled system can keep part of its memory. As low frequency variability is associated with close ocean–atmosphere interaction, we suggest that interannual SST anomaly information could drive winds that help HC to recover; and HC evolution can alter SST via upwelling changes that lead to recovery of SST skill.

To investigate possible long-term changes in predictability, the dynamical predictions were separated into two subsets, initialized during the 1970s and 1980s, respectively, with each subset containing at least two warm ENSO events. (Reliable wind data needed for predictions for earlier decades were not available.) Taking all seasons into account, correlation skill was generally higher in the 1980s than in the 1970s. Large differences in the seasonality of the predictions between the two decades were also found; the spring decay in SST′ correlation was large and coherent in the 1970s, but small and not so coherent for predictions initialized during the 1980s. Similar results were obtained for predictions made using simple persistence of observed SST anomalies. For HC′ predictions, correlations show a winter barrier in the 1970s that is not evident in the 1980s. For one decade, the sample size for these seasonally separated correlations is small, so the significance of the individual results is low. However, the consistency of the results from different datasets strongly suggests that the decadal differences are real.

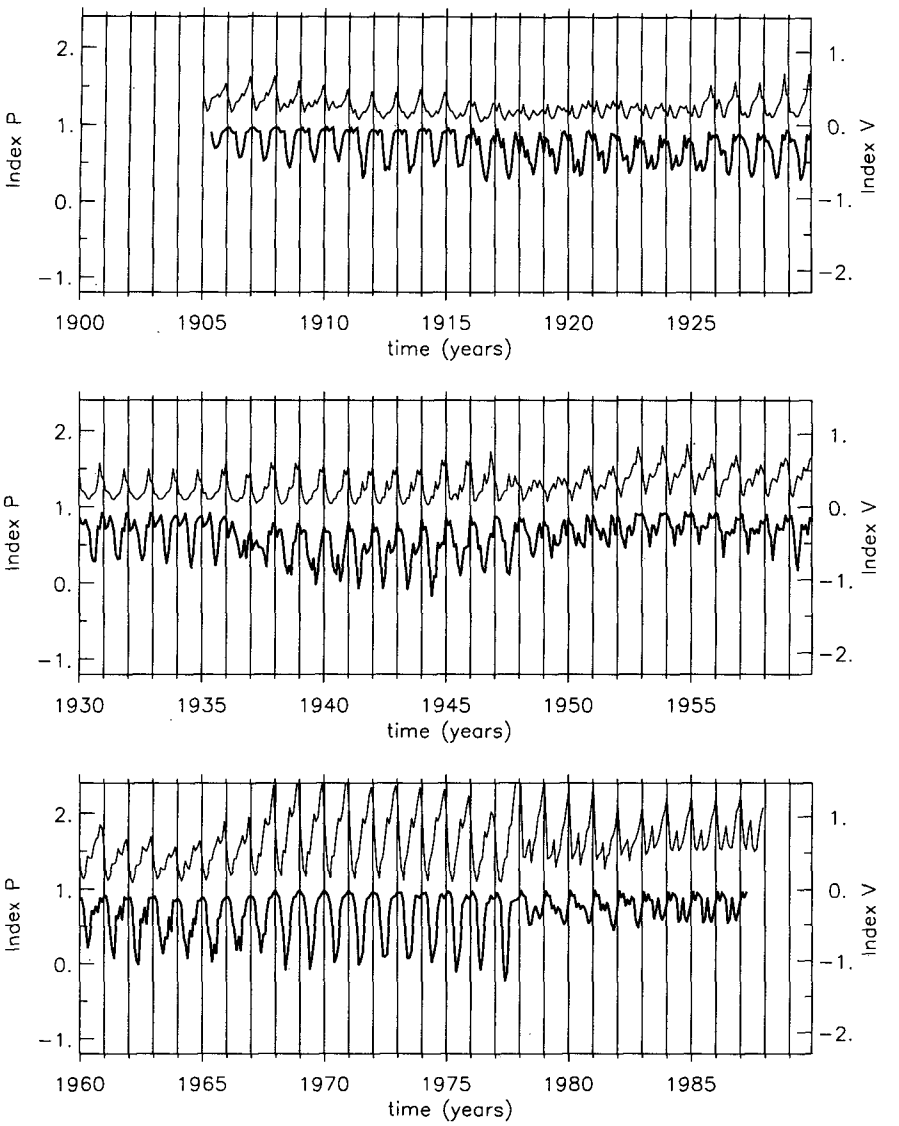

FIG. 12. Time evolution of the persistence (3-month lead) correlation index P (thick curve) and the variance index V (thin curve) during this century (see text for definitions). Vertical lines correspond to the start of each year. The scale for P is on the left, and on the right (displaced upward) for V.

In the 1970s there is a strong spring barrier in SST′ prediction skill, for various skill measures, and a strong minimum in spring SST′ variance. By contrast, in the 1980s there is no obvious barrier and no clear variance minimum. The coherent relationship between the seasonality in SST prediction skill and variance (which is dominated by El Niño) suggests that they are connected by the degree of phase locking of El Niño to the annual cycle. When phase locking is strong (e.g., if the transition phase consistently occurs in a particular season) then there is a minimum in variance associated with that season, and predictions show a strong seasonal barrier (i.e., a sharp decline in skill when forecasting conditions for that season). Thus, El Niño predictive skill may depend substantially on the degree of phase-locking of El Niño to the annual cycle, as well as on stability conditions associated with the background seasonal cycle.

Motivated by the variations found in the skill of El Niño predictions during the 1970s and 1980s, the seasonality and predictability of interannual SST anomalies in the tropical Pacific were investigated using SST data from 1900 to 1990. The interdecadal behavior of two seasonally varying indices was calculated. Index P measures 3-month lead persistence correlation skill within a running decadal window: large dependence of P on month-of-year indicates a seasonal prediction barrier. Index V similarly measures variance within the

decadal window: large seasonal changes in V occur when anomalies are strongly phaselocked to the annual cycle. Changes in P and V reveal interdecadal variability in predictive skill and in seasonal phase locking of the El Niño cycle. In most of this century there is moderate to strong locking of interannual variability to the seasonal cycle, with winter maxima in V and P followed by rapid declines. This type of behavior was most pronounced in the 1970s. Seasonality is relatively weak and irregular in the late 1910s and early 1920s, in the 1950s, and in the 1980s.

These interdecadal results should be treated with caution, as data coverage through this century is very variable. The indices suggest, however, that characteristics such as seasonal phase locking do vary on a decadal timescale, and that there may consequently be decadal fluctuations in predictability. The nature and causes of such changes require further investigation.

Acknowledgments. Thanks are due to Chris Folland, Mike Jackson, and the Climate Data group at the Hadley Centre for creating and supplying the GISST dataset, to James Stricherz at The Florida State University for supplying wind data for the predictions, and to anonymous referees for their constructive comments.

REFERENCES

Balmaseda, M. A., D. L. T. Anderson, and M. K. Davey, 1994: ENSO prediction using a dynamical ocean model coupled to statistical atmospheres. *Tellus,* **46A,** 497–511.

Battisti, D. S., 1988: Dynamics and thermodynamics of a warming event in a coupled tropical atmosphere–ocean model. *J. Atmos. Sci.,* **45,** 2889–2919.

Blumenthal, M. B., 1991: Predictability of a coupled ocean–atmosphere model. *J. Climate,* **4,** 766–784.

Gill, A. E., and E. M. Rasmusson, 1983: The 1982–83 climate anomaly in the equatorial Pacific. *Nature,* **306,** 229–234.

Goldenberg, S. D., and J. J. O'Brien, 1981: Time and space variability of tropical Pacific wind stress. *Mon. Wea. Rev.,* **109,** 1190–1207.

Goswami, B. N., and J. Shukla, 1991: Predictability of a coupled ocean–atmosphere model. *J. Climate,* **4,** 3–22.

Kerr, R. A., 1992: Unmasking a shifty climate system. *Science,* **225,** 1508–1510.

Kousky, V. E., and A. Leetmaa, 1989: The 1986–87 Pacific warm episode: Evolution of oceanic and atmospheric anomaly fields. *J. Climate,* **2,** 254–267.

Latif, M., and N. E. Graham, 1992: How much predictive skill is contained in the thermal structure of an oceanic GCM? *J. Phys. Oceanogr.,* **22,** 951–961.

——, T. P. Barnett, M. A. Cane, M. Flügel, N. E. Graham, H. von Storch, J.-S. Xu, and S. E. Zebiak, 1994: A review of ENSO prediction studies. *Climate Dyn.,* **9,** 167–179.

McCreary, J. P., and D. L. T. Anderson, 1991: An overview of coupled ocean–atmosphere models of El Niño and the Southern Oscillation. *J. Geophys. Res.,* **96,** 3125–3150.

Neelin, J. D., M. Latif, and F.-F. Jin, 1994: Dynamics of coupled ocean–atmosphere models: The tropical problem. *Annu. Rev. Fluid Mech.,* **26,** 617.

Parker, D. E., C. K. Folland, A. Bevan, M. N. Ward, M. Jackson, and K. Maskell, 1994: Marine surface data for analysis of climatic fluctuations on interannual to century timescales. *Natural Climate Variability on Decade to Century Time Scales,* D. G. Martinson, K. Bryan, M. Ghil, M. M. Hall, T. R. Karl, E. S. Sarachik, S. Soroostian, and L. F. Talley, Eds., National Academy Press.

Rasmusson, E. M., and T. H. Carpenter, 1982: Variations in tropical sea surface temperature and surface wind fields associated with the Southern Oscillation/El Niño. *Mon. Wea. Rev.,* **110,** 354–384.

Trenberth, K. E., 1990: Recent observed interdecadal climate changes in the Northern Hemisphere. *Bull. Amer. Meteor. Soc.,* **71,** 988.

——, and J. W. Hurrell, 1994: Decadal atmosphere–ocean variations in the Pacific. *Climate Dyn.,* **9,** 303–319.

Wang, B., 1995: Interdecadal changes in El Niño in the last four decades. *J. Climate,* **7,** 267–285.

Webster, P. J., and S. Yang, 1992: Monsoon and ENSO: Selectively interactive systems. *Quart. J. Roy. Meteor. Soc.,* **118,** 877–926.

Woodruff, S. D., R. J. Slutz, R. L. Jenne, and P. M. Steurer, 1987: A comprehensive ocean-atmosphere data set. *Bull. Amer. Meteor. Soc.,* **69,** 1239–1250.

Xue, Y., M. A. Cane, S. E. Zebiak, and M. B. Blumenthal, 1994: On the prediction of ENSO: A study with a low-order Markov model. *Tellus,* **46A,** 512–528.

Zebiak, S. E., and M. A. Cane, 1987: A model El Niño–Southern Oscillation. *Mon. Wea. Rev.,* **115,** 2262–2278.